Cell

The ClpXP Protease Unfolds Substrates Using a Constant Rate of Pulling but Different Gears

Maya Sen,[1,2,9] Rodrigo A. Maillard,[1,3,9] Kristofor Nyquist,[3,4,9] Piere Rodriguez-Aliaga,[1,3,4] Steve Pressé,[8] Andreas Martin,[3,5,*] and Carlos Bustamante[1,2,3,5,6,7,*]
[1]Jason L. Choy Laboratory of Single-Molecule Biophysics
[2]Department of Chemistry
[3]QB3 Institute
[4]Biophysics Graduate Group
[5]Department of Molecular and Cell Biology
[6]Department of Physics
[7]Howard Hughes Medical Institute
University of California, Berkeley, Berkeley, CA 94720, USA
[8]Department of Physics, Indiana University-Purdue University, Indianapolis, IN 46202, USA
[9]These authors contributed equally to this work
*Correspondence: a.martin@berkeley.edu (A.M.), carlos@alice.berkeley.edu (C.B.)
http://dx.doi.org/10.1016/j.cell.2013.09.022

SUMMARY

ATP-dependent proteases are vital to maintain cellular protein homeostasis. Here, we study the mechanisms of force generation and intersubunit coordination in the ClpXP protease from *E. coli* to understand how these machines couple ATP hydrolysis to mechanical protein unfolding. Single-molecule analyses reveal that phosphate release is the force-generating step in the ATP-hydrolysis cycle and that ClpXP translocates substrate polypeptides in bursts resulting from highly coordinated conformational changes in two to four ATPase subunits. ClpXP must use its maximum successive firing capacity of four subunits to unfold stable substrates like GFP. The average dwell duration between individual bursts of translocation is constant, regardless of the number of translocating subunits, implying that ClpXP operates with constant "rpm" but uses different "gears."

INTRODUCTION

ATP-dependent proteases of the AAA+ family play crucial roles for the maintenance of cellular protein homeostasis, including the clearance of misfolded, aggregated, or damaged proteins, as well as the disassembly of large macromolecular complexes (King et al., 1996; Hanson and Whiteheart, 2005; White and Lauring, 2007). These multimeric molecular machines encounter unique chemical and mechanical challenges during their task of protein unfolding and polypeptide translocation. First, the motor must translocate along a heterogeneous and flexible polypeptide track composed of amino acids with highly diverse chemical and physical properties. Second, the motor must unravel a diverse array of folded protein domains with a range of stabilities that represent mechanical obstacles along the track. Understanding how ATP-dependent proteases perform these tasks will shed light on their general principles of operation and their mechanochemistry, specifically how they convert chemical energy from ATP hydrolysis to mechanical work and how individual subunits are coordinated.

Escherichia coli ClpXP is a well-characterized model system to investigate the operating principles of ATP-dependent proteases (Baker and Sauer, 2012). Homohexameric rings of the ClpX ATPase associate with the peptidase ClpP to form the ClpXP protease. ClpP is made up of two coaxially stacked homoheptameric rings with proteolytic active sites sequestered inside an internal cavity (Gottesman et al., 1998). To achieve specific protein degradation, ATP-bound ClpX recognizes protein substrates with certain degradation tags (Baker and Sauer, 2012) and uses cycles of ATP hydrolysis to unfold and translocate these substrates through its central pore into ClpP for proteolysis (Figure 1A) (Baker and Sauer, 2006). Conserved loops (pore-1 loops) that protrude from every ClpX subunit into the central pore have been proposed to directly contact the substrate (Martin et al., 2008a), and ATP-dependent conformational changes of these subunits are thought to unravel folded domains and propel the polypeptide through the central channel (Glynn et al., 2009).

Previous mutagenesis studies have suggested that the ClpX subunits contribute additively to substrate processing and that the power stroke for translocation may be generated by ATP hydrolysis in one subunit at a time (Martin et al., 2005), supporting a probabilistic mechanism of ring subunit coordination (Glynn et al., 2009; Stinson et al., 2013). Using optical tweezers, we and others provided direct demonstration that ClpX transforms the energy of ATP hydrolysis into mechanical force, and that polypeptide translocation occurs in cycles composed of a dwell phase, during which the substrate does not move, and a burst phase, during which ClpXP near-instantaneously translocates

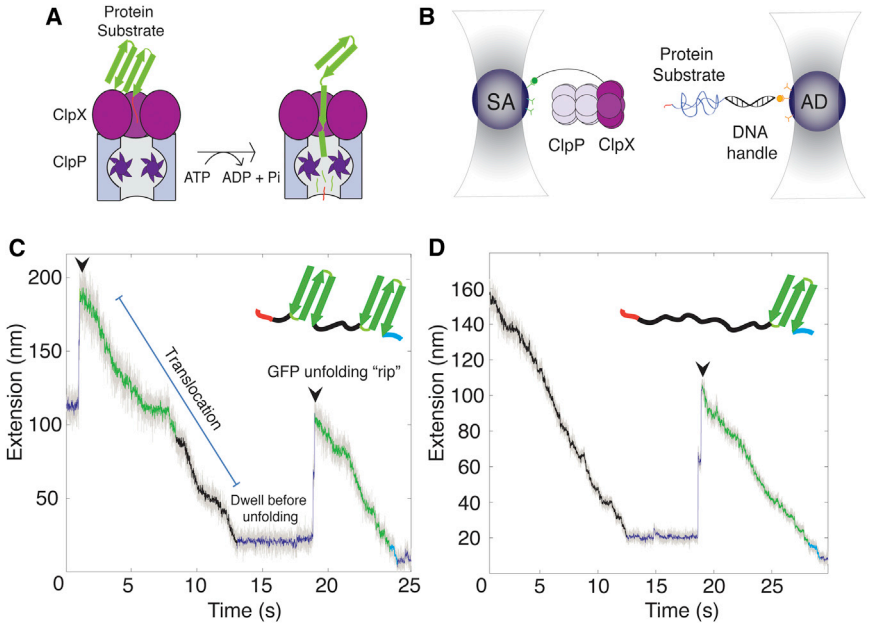

Figure 1. Single-Molecule Experimental Constructs

(A) Cartoon depicting protein unfolding and polypeptide translocation by ClpXP.

(B) Experimental geometry of dual-trap optical tweezers assay (not to scale). Biotinylated ClpX was immobilized on streptavidin-coated beads (SA). The DNA-tethered substrate was immobilized on the surface of beads coated with anti-digoxigenin antibodies (AD).

(C and D) Single-molecule trajectories of substrate processing by ClpXP at 1 mM ATP and forces ranging from 6 to 12 pN. GFP unfolding events are indicated by arrows and followed by translocation of unfolded polypeptide. Substrates are composed of GFP moieties (green) fused to titin^{CM} and a C-terminal ssrA tag (black and red, respectively), as well as an N-terminal ybbR tag (light blue) for attachment to the bead. Raw data (2.5 kHz in gray) were filtered and decimated to 100 Hz (green, black, and blue lines).

the polypeptide by a certain length (Aubin-Tam et al., 2011; Maillard et al., 2011).

Our previous findings motivated us to perform a mechanochemical characterization of ClpXP and to address the following questions: do all ATPase subunits participate during substrate translocation and what is the mechanism of coordination within the hexameric ring? Is the coordination among subunits different during protein unfolding versus processive translocation of an unstructured polypeptide? Which transitions determine the timing of the mechanochemical cycle? How is the chemical energy from ATP hydrolysis coupled to the mechanical cycle that drives translocation?

To address these mechanistic questions, we utilized single-molecule optical tweezers, which allow us to probe the motor's mechanochemical coupling by applying external forces while simultaneously perturbing the chemical transitions of the ATPase cycle. These studies provided us with several important findings. We determined that to stall the motor during polypeptide translocation ATP hydrolysis in at least three of the six subunits must be inhibited. We found that a process not coupled to ATP binding sets the dwell duration between translocation bursts and that the burst size depends on the number of hydrolyzing ClpX subunits in the hexamer. This number distributes between two, three, and four subunits and their relative occurrence changes as ATP is varied from K_m to saturation. During a burst, the near-simultaneous firing and translocation by two, three, or four subunits occurs in a coordinated fashion before the hexamer starts a new mechanochemical cycle. We find that these highly coordinated power strokes occur upon phosphate release and that they play a crucial role in the ability of ClpXP to denature kinetically stabilized protein substrates like GFP. Contrary to previously proposed probabilistic models (Martin et al., 2005; Glynn et al., 2009; Stinson et al., 2013), our results establish a high degree of coordination between ATP-bound subunits in the ClpX hexamer. ClpX seems to employ a novel mechanism of translocation that significantly deviates from canonical motor mechanisms, demonstrating how specialized molecular machines have been optimized to carry out their specific tasks.

RESULTS

Single-Molecule Assays

We used dual-trap optical tweezers in passive mode (constant trap position, variable force) to monitor a single ClpXP complex as it unfolds and translocates protein substrates in an ATP-hydrolysis-dependent manner. ClpXP was immobilized on one polystyrene bead and the ssrA-tagged protein substrate was attached to another. Each bead was held in an optical trap, and a tether formed between the beads once ClpXP engaged its substrate (Figure 1B) (Maillard et al., 2011). Two fusion substrates of the green fluorescent protein (GFP) and a permanently unfolded variant of the I27 domain of titin (titin^{CM}) were used (C to N terminus): ssrA-titin^{CM}-GFP-(titin^{CM})$_2$-GFP and ssrA-(titin^{CM})$_4$-GFP (Figures 1C and 1D, respectively). Substrate unfolding was measured as a sudden gain in extension of the tether (rip), whereas polypeptide translocation was monitored as the gradual decrease of extension with time. Because ClpXP cannot efficiently unfold GFP at ATP concentrations below 200 μM, the second substrate allowed the measurement of extended translocation of titin domains without the requirement for GFP unfolding.

Phosphate Release Is the Force-Generating Step in the ClpXP ATPase Cycle

To probe the relationship between the generation of mechanical work and the ATPase cycle, which includes initial ATP binding, tight binding, hydrolysis, and the release of ADP and inorganic phosphate (see scheme in Figure 2A), we studied ClpXP in the presence of various concentrations of ATP, ADP, and inorganic

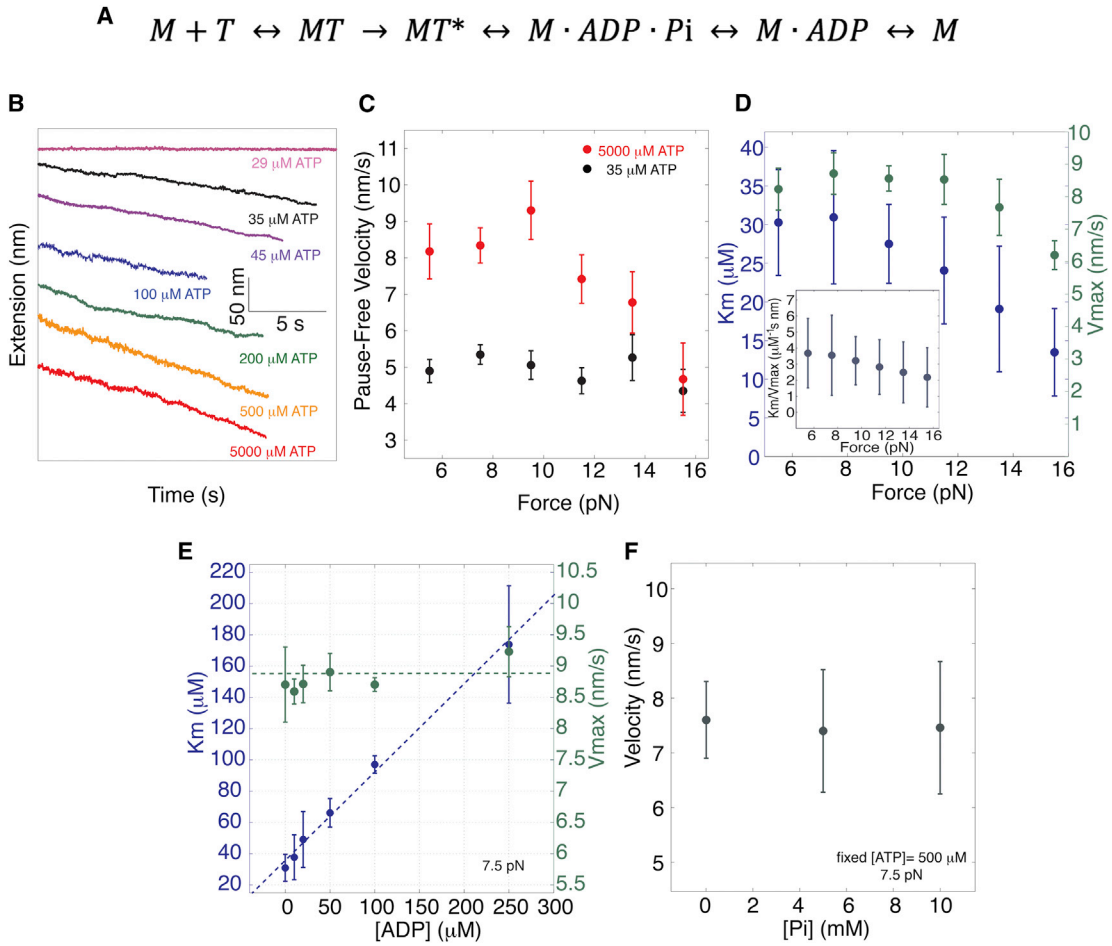

Figure 2. Effects of ATP, ADP, and Pi on Translocation

(A) General scheme depicting a motor (M) that binds to one ATP molecule (T), undergoes a tight binding transition, and hydrolyzes ATP, followed by the release of inorganic phosphate (Pi) and ADP.

(B) Representative trajectories for translocation of the titin^{CM} moiety of the fusion substrates measured between 6 and 12 pN at different ATP concentrations with ATP regeneration system (ATP/RS). The trajectories are offset for clarity.

(C) Pause-free velocity of translocation (mean ± SEM) as a function of external force at 5 mM ATP (red symbols) and 35 μM ATP (black symbols).

(D) K_m (blue) and V_{max} (green) are plotted against force. Inset: K_m/V_{max} ratio plotted for forces between 5 to 15 pN. Error bars are from the fits (SEM).

(E) K_m (blue) and V_{max} (green) plotted against ADP concentration at 7.5 pN. Error bars are from the fits (SEM).

(F) Pause-free velocity of translocation (mean ± SEM) plotted as a function of phosphate concentration [Pi] at 7.5 pN with a fixed [ATP] (see also Figure S1).

phosphate (Pi). First, we explored the effect of the ATP concentration on translocation and thereby focused solely on the titin^{CM} regions of the fusion substrate in order to minimize potential effects of amino acid sequence differences between titin^{CM} and GFP (Figure 2B). Translocation was punctuated by rare pauses that are typically longer than 1 to 2 s (Experimental Procedures). Pauses were previously shown to be in kinetic competition with translocation and therefore off the main translocation pathway (Maillard et al., 2011). Pause-free translocation as a function of the ATP concentration followed a general Michaelis-Menten behavior $v = V_{max}[ATP]/([ATP] + K_m)$ (Figure S1A available online; Extended Experimental Procedures).

To determine whether ATP binding is the force-generating step, we examined how the translocation velocity depends on force at various ATP concentrations. If ATP binding is coupled to force generation, then conditions in which ATP binding becomes rate limiting should make the conformational changes that drive translocation also rate limiting. In this case, the motor velocity would be highly sensitive to the applied external load. However, we found that the translocation velocity of ClpX is largely insensitive to opposing mechanical forces at low ATP concentrations (Figure 2C, black symbols). In contrast, at saturating ATP concentrations (≥500 μM) and opposing forces between 12 and 20 pN, the force-generating step has become rate limiting and ClpX translocation is force sensitive (Figure 2C, red symbols). These results clearly indicate that ATP binding does not power substrate translocation.

Next, we analyzed the force dependence of the Michaelis-Menten parameters V_{max} and K_m to determine where the force-generating step may be located in the nucleotide-hydrolysis

cycle. The Michaelis-Menten fits to our data revealed that both V_{max} and K_m decrease with the applied load (Figure 2D), but the K_m/V_{max} ratio remains force insensitive (Figure 2D, inset). A force-independent K_m/V_{max} is consistent with our conclusion that ATP binding does not power translocation and indicates that the force-generating step must occur after the first irreversible transition connected to ATP binding (Chemla et al., 2005; Keller and Bustamante, 2000; Visscher et al., 1999). This irreversible transition is most likely the tight binding of ATP, as previously seen in other ring ATPases such as the F1-ATPase and the φ29 DNA packaging motor (Adachi et al., 2007; Chemla et al., 2005; Oster and Wang, 2000).

The results above leave only ATP hydrolysis, ADP release, or Pi release as possible transitions that may couple to the force-generating step (Figure 2A). ATP hydrolysis is unlikely to power translocation, because the small rotation of the terminal phosphate upon hydrolysis does not provide the free energy change required for the power stroke (Oster and Wang, 2000). To investigate the role of product release in the mechanochemical cycle, we varied the concentrations of ADP and Pi. The effect of increasing ADP concentrations on the pause-free velocity of ClpXP obeyed a Michaelis-Menten model of competitive inhibition (Figure S1B). The apparent K_m for ATP was seen to increase linearly with [ADP] according to $K_m = K_m^0(1 + [ADP]/K_i)$, whereas V_{max} remained constant (Figure 2E) (Segel, 1975). Our results are consistent with the known role of ADP as a competitive inhibitor of the ClpX motor (Burton et al., 2003). In contrast, increasing [Pi] from 5 μM to 10 mM did not affect the translocation velocity (Figure 2F), indicating that Pi release is a largely irreversible transition.

To discriminate between the possible roles of ADP and Pi release in the mechanism of force generation, we estimated the free energy changes of these events based on their respective dissociation constants and compared them to the observed maximum work performed by ClpXP. Using an estimated step size of 1 nm (Glynn et al., 2009; Aubin-Tam et al., 2011; Maillard et al., 2011) and a stall force of at least 20 pN, ClpX subunits perform a near-maximum work of 20 pN × 1 nm or ΔG = 4.8 k_BT when taking 1 nm steps near stall. Using K_i = 33 μM as a dissociation constant for ADP (Figure 2E; Extended Experimental Procedures), the change in free energy from ADP release is $\Delta G_D \sim 1.8\ k_BT$ (at [ADP] = 5 μM) and thus is insufficient to account for the work performed by ClpXP. In contrast, phosphate release is considered irreversible because the velocity is unaffected even at high [Pi] (10 mM). Therefore, the dissociation constant for phosphate release must be $K_d >> 10$ mM, with a corresponding change in free energy of $\Delta G_P >> 7.6\ k_BT$ (for $[P_i]$ = 5 μM). Phosphate release would thus provide sufficient energy to power the work produced by ClpXP in every translocation step and is the most likely candidate for the force-generating step of the motor.

ATPγS Dependence of Pause Density and Pause Duration Reveals High Intersubunit Coordination during Translocation

Effective unfolding and/or translocation of protein substrates by ClpX may require the participation of multiple subunits in the hexamer (Martin et al., 2008a). We therefore sought to characterize how individual subunits coordinate their ATP hydrolysis activities around the ring. To this end, we slowed down the hydrolysis in a given subunit by using the ATP analog ATPγS, which ClpX hydrolyzes ~90 times slower than ATP (Figure S2; Extended Experimental Procedures) and determined how binding of this analog affected the polypeptide translocation by the remaining ATP-bound subunits in the ring. We held [ATP] fixed at 500 μM and varied [ATPγS] from 0 to 250 μM. In the presence of ATPγS, we observed pauses longer than 1 s, which were extremely rare in the presence of ATP alone, and we attributed these long pauses to ATPγS-bound ClpX subunits (Figure 3A). Furthermore, the relationship between the average translocation velocity and the ATPγS concentration decreased in a nonlinear fashion due to these long pauses. The trend could be fitted well to a modified Hill equation with a Hill coefficient $n_{ATP\gamma S}$ = 1.5 ± 0.3 (SEM) (Figure 3B), indicating that more than one ATPγS binding to the ring is necessary to induce a long pause during translocation.

We observed that the pause density (PD), i.e., the number of pauses per nm of translocated polypeptide, increased with the ATPγS concentration, indicating that the entry into a pause was caused by the binding of ATPγS to the ring (Figure 3C; Experimental Procedures). The maximum PD, PD_{max}, reflects the existence of an ATPγS concentration at which the motor has nearly 100% probability of binding the minimum number of ATPγS molecules required to stall translocation. Accurate pause detection became difficult at high concentrations of ATPγS (greater than ~200–250 μM). To calculate PD_{max}, we plotted the inverse of the ATPγS concentration against the inverse of PD and estimated a PD_{max} of ~0.5 nm^{-1} (Figure 3C). Thus, the motor has a 50% probability of entering a pause at [ATPγS] = 200 μM (Figure 3C, inset). Using a $K_{m,ATP\gamma S}$ = 29 μM as an upper bound for the ATPγS dissociation constant (because k_{cat} has little contribution), we calculated that the probability of having three or more ATPγS bound to the ring at [ATPγS] = 200 μM is ~0.44 (see Extended Experimental Procedures), very close to the observed 50% probability of the motor entering into an analog-induced pause (Figure 3C, inset). We conclude that at least three molecules of ATPγS are required to bind to the ring in order to stall translocation and induce a pause. Consequently, intersubunit coordination around the ring does not require the involvement of all ATP-binding-competent subunits.

One of two different processes is likely to dictate the kinetics of exit from a pause: (1) the dissociation or (2) the hydrolysis of ATPγS. To distinguish between these alternatives, we compared the ATPγS hydrolysis rate with the average duration of the ATPγS-induced pauses. Hydrolysis of a single ATPγS molecule takes ~10 s in the presence of titin^{CM}-ssrA (k_{cat} of ~6 min^{-1} $hexamer^{-1}$), which is ~90 times slower than the rate of ATP hydrolysis under identical conditions (Figure S2; Extended Experimental Procedures). Because the observed mean pause durations are significantly shorter than the time for ATPγS hydrolysis, we conclude that they primarily reflect the off-rate of ATPγS. Interestingly, the mean pause durations increased from ~1.5 to ~2.5 s as the ATPγS concentration was increased from 50 to 250 μM (Figure 3D) (see Experimental Procedures). Thus, the exit from a pause takes longer as the motor loads

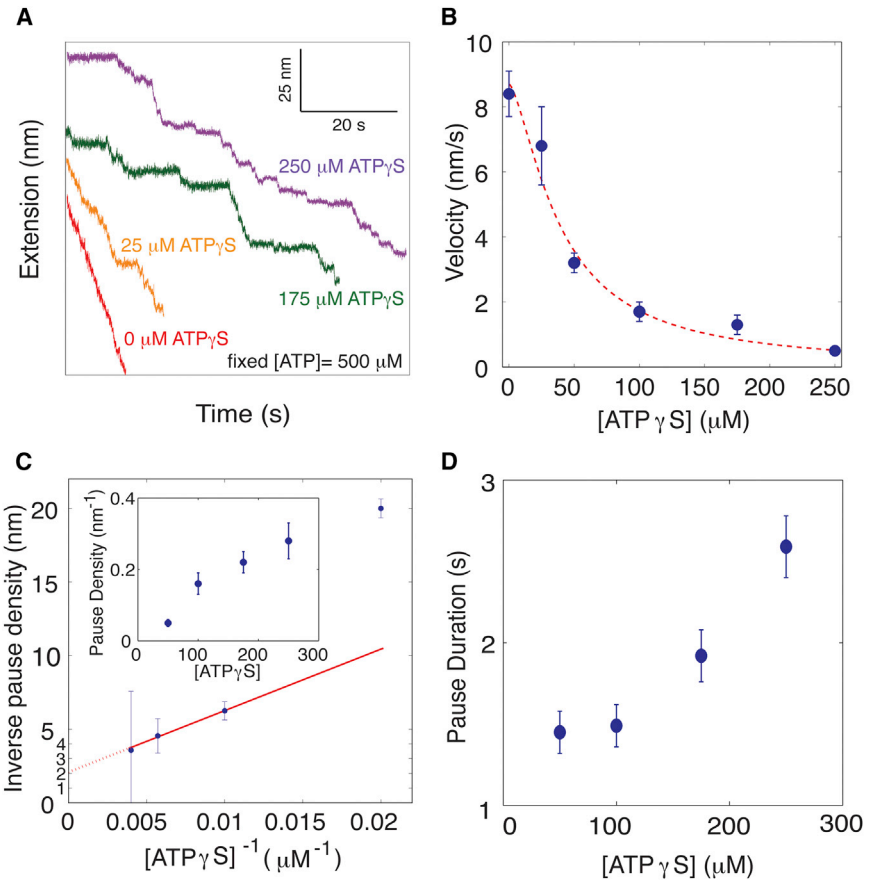

Figure 3. ATPγS Induces Long-Lived Pauses

(A) Representative trajectories for forces between 6 and 12 pN were measured with increasing [ATPγS] at fixed [ATP]. Trajectories are offset for visual clarity.

(B) Translocation rate (mean ± SEM) plotted against [ATPγS], with the fit shown in red.

(C) Inverse density of ATPγS-induced pauses (mean ± SEM) plotted against the inverse of [ATPγS], with the linear fit shown in red. Inset: pause density (mean ± SEM) plotted as a function of [ATPγS].

(D) Pause duration (mean ± SEM) as a function of [ATPγS] (see also Figure S2).

with an increasing number of ATPγS molecules, most likely reflecting the extra time required to eject multiple ATPγS molecules until just two ATPγS remain bound to the ring.

Effect of [ATP] on Burst Sizes and Dwell Durations

The observation that the motor can maintain its operation even when one or two analog molecules are bound to the ClpX ring led us to investigate in greater detail the mechanism by which subunits communicate with each other around the ring. Previous single-molecule studies showed that ClpXP translocates polypeptide in bursts of 1, 2, and 3 nm (Maillard et al., 2011). Based on the ClpX crystal structure that shows an ~1 nm displacement between the pore-1 loops in ATP-bound and empty states (Glynn et al., 2009), a 1 nm step was thought to reflect the basic power stroke of a single ClpX subunit (Aubin-Tam et al., 2011; Maillard et al., 2011). Accordingly, the 2 and 3 nm bursts were interpreted as the near-simultaneous firing of two and three ClpX subunits, respectively (Maillard et al., 2011). An important remaining question is what mechanism individual ATPase subunits use to coordinate their translocation activities at any given ATP concentration. To address this point, we analyzed how different ATP concentrations affected the distributions of burst sizes and dwell times (Figure 4A).

At [ATP]>>K_m, burst sizes of 2–4 nm were observed at opposing forces between 6 and 15 pN (Figures 4B and S3; Extended Experimental Procedures). The distribution of burst sizes has a maximum at ~3 nm, with a correspondingly lower number of ~2 and ~4 nm bursts. In contrast, when ATP binding is near rate limiting ([ATP] = 35 μM), ClpXP translocates mostly in 2 or 3 nm bursts, and bursts of 4 nm are completely absent (Figure 4B, red histogram).

Next, we analyzed the duration of the cycle time (the sum of the dwell and burst phase duration) at various ATP concentrations to better understand the translocation mechanism of this motor. Surprisingly, we observed that the mean cycle time has no apparent dependence on [ATP]. We found that the mean duration of the dwell phase $<\tau>$ is 350 ± 20 ms in the range between 35 μM and 5 mM (Figure 4C). In addition, the duration of the burst phase contributes to less than ~3% of the cycle time and has a mean duration of less than ~10 ms. In this range of nucleotide concentrations, the motor translocation rate approximately doubles from 5 to 9 nm/s. Consequently, the observed change in translocation rate is not due to changes in the mean cycle time, but rather to a systematic increase in motor burst size with increasing [ATP].

To obtain insight into the molecular processes that occur during the dwell time, we calculated the kinetic parameter n_{min}, which is defined as the ratio of the squared mean of dwell times over the variance of the dwell times, $n_{min} = <\tau>^2/(<\tau>^2 - <\tau>^2)$ (Moffitt et al., 2006; Schnitzer and Block, 1995). It has been shown that this parameter provides a strict lower bound to the number of rate-limiting events during the dwell phase (Moffitt et al., 2006). We sought to understand how the number of rate-limiting events (n_{min}) changes with the ATP concentration. At saturating and near-K_m concentrations of ATP, we measured n_{min} = 2.1 ± 0.4 and 2.0 ± 0.6 (SEM), respectively, suggesting that for both conditions there are at least two rate-limiting transitions in the dwell leading up to the burst phase. Similar values of n_{min} = 1.9 ± 0.6 were obtained at the intermediate ATP concentrations of 100 and 200 μM. Therefore, at least two processes—not associated with ATP binding—control the duration of the dwell in the [ATP] range between 35 μM (near K_m) and 5 mM (saturating).

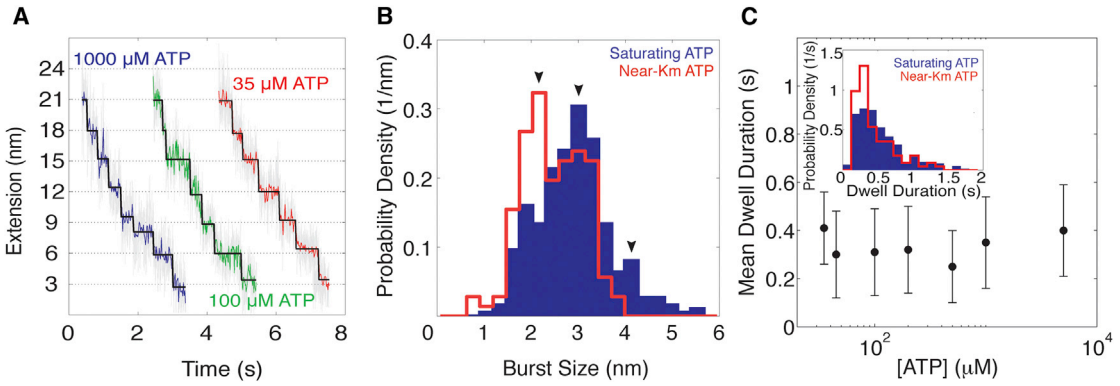

Figure 4. Effect of ATP Concentration on Burst Size and Dwell Duration

(A) Representative trajectories of ClpXP translocating substrate in 3 nm steps at 10–14 pN and different ATP concentrations. Raw data were filtered and decimated to 1,250 (in gray) or 50 Hz (in red, blue, green). t test fits to the data are shown in black.

(B) Burst size distributions for ATP concentrations near K_m (red) and saturating ATP (blue).

(C) Mean dwell duration (±SEM) plotted against [ATP]. Inset: dwell-time distribution for near-K_m conditions (red) and saturating ATP (blue) (see also Figure S3).

Altogether, these results suggest a mechanism of translocation that is strikingly different from those of other motors. The well-characterized DNA packaging motor of bacteriophage φ29 exhibits a variable, ATP-concentration-dependent dwell time followed by a constant, ATP-concentration-independent burst size of 10 bp, which reflects a high degree of coordination among the ring subunits that must all load ATP before the motor can initiate translocation (Chistol et al., 2012; Moffitt et al., 2009). In sharp contrast, ClpXP exhibits an ATP-concentration-independent cycle time, during which a variable number of ATP molecules bind to the motor, resulting in a distribution of burst sizes.

ClpXP Requires Four Highly Coordinated Power Strokes for Successful Unfolding of GFP

Our findings that ClpX translocates with variable burst sizes and that the burst-size distribution is ATP concentration dependent raises two important questions about the mechanism by which the motor successfully unfolds protein substrates. First, how are the power strokes of individual subunits coordinated during protein unfolding? And second, what is the kinetic competition between the motor translocation bursts and the substrate's resistance to unravel and its tendency to refold? To answer these questions, we quantified how variations in ATP concentration (and therefore in translocation burst sizes) affect the ability of the motor to unfold GFP. We found that reducing the ATP concentration decreased the probability of GFP unfolding by ClpXP nonlinearly from a maximum of 0.6 when [ATP] ≥500 μM to less than 0.1 when [ATP] ≤50 μM (Figure 5A).

The nonlinear relationship between GFP unfolding probability and ATP concentration suggests that GFP unfolding requires the coordinated and near-simultaneous ATP hydrolysis of multiple ClpX subunits in the ring. In order to elucidate the coordination mechanism by which ClpXP successfully unfolds GFP, we characterized the intermediates observed during GFP unfolding. Unraveling of GFP from the C terminus proceeded via two transient intermediates with mean lifetimes of 45 ± 10 and 130 ± 15 ms (Figures 5B, S4A, and S4B; Supplemental Information). By using the wormlike chain (WLC) model of polymer elasticity (Bustamante et al., 1994), we estimated that the transition from the folded state "F" to the first intermediate "I" (F→I) has a contour length increase $\Delta Lc^{F\rightarrow I}$ of 8.3 ± 0.4 nm (SEM) corresponding to the extraction of β strand 11 (β11) from the GFP barrel. The second transition from "I" to the second intermediate "II" (I→II) has a $\Delta Lc^{I\rightarrow II}$ of 31.2 ± 0.8 nm and most likely corresponds to the unfolding of β strands 10 through 7. The last transition from "II" to the unfolded state "U" (II→U) has a $\Delta Lc^{II\rightarrow U}$ of 42.2 ± 0.8 nm and reflects the unraveling of the remaining six β strands, as described previously (Maillard et al., 2011) (Figures 5C and S4C–S4I; Extended Experimental Procedures). The total contour length increase $\Delta Lc^{F\rightarrow U}$ (= $\Delta Lc^{F\rightarrow I}$ + $\Delta Lc^{I\rightarrow II}$ + $\Delta Lc^{II\rightarrow U}$) of 82.8 ± 3.2 nm is in agreement with the expected value for the complete unfolding of GFP (Figure S4C; Supplemental Information).

At [ATP] ≤ 200 μM, we detected small unfolding and refolding events before ClpXP completely unraveled GFP (Figure 5D). The change in contour length during the reversible unfolding and refolding events is similar to $\Delta Lc^{F\rightarrow I}$, suggesting that these events most likely correspond to the extraction and quick refolding of β11. Analysis of these reversible transitions revealed that β11 snaps back into the GFP barrel with a mean refolding time constant ~240 ms at forces between 7 and 9 pN (Figures S4J and S4K; Supplemental Information). These results provide direct experimental evidence of the molecular tug-of-war between the motor, attempting to unravel folded structures, and a substrate with a strong tendency to refold. Hence, protein-unfolding machines have to perform not only the thermodynamic function of mechanically destabilizing the native state, but also the kinetic task of quickly capturing the unstructured polypeptide before it can refold.

When [ATP] >> K_m, ClpXP is able to move in bursts of 4 nm during a single translocation cycle. Such coordinated translocation is sufficient to trap most of the dislodged β11 and prevent its refolding. These observations indicate that the efficient unfolding of GFP by ClpXP requires not only a 4 nm burst, but also this burst to occur faster than the refolding time of β11 (<240 ms). Using the distribution of burst size and dwell duration determined

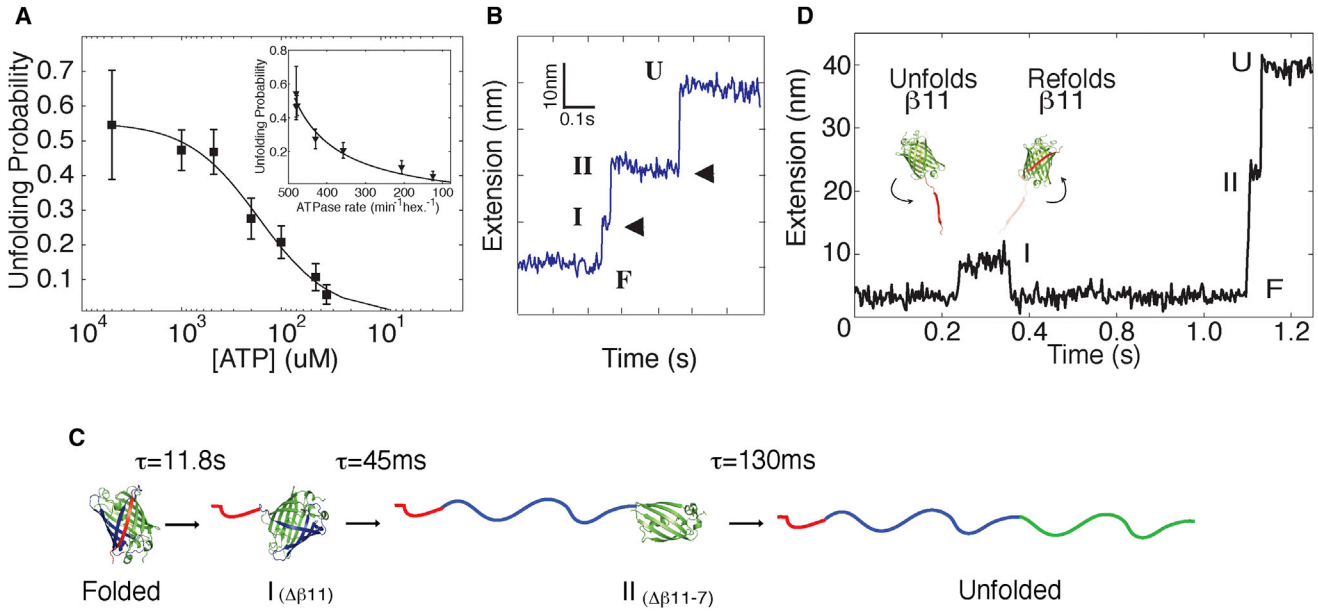

Figure 5. GFP Unfolding Mechanism

(A) Probability of GFP unfolding as a function of [ATP] and ATPase rate (inset). Error bars are ± SEM.

(B) GFP unfolding events display two intermediates at 300 Hz.

(C) Mechanism of GFP unfolding by ClpXP at [ATP] >> K_m.

(D) Trajectory at [ATP] = 200 μM illustrating the ClpXP-induced unfolding and refolding of β11 (see also Figure S4).

here, we estimated the probability of ClpXP taking a 4 nm burst in less than 240 ms to be on average 0.031 (0.018–0.046). This result indicates that ClpXP must pass through ~33 translocation cycles before it can unfold GFP and trap the first intermediate for subsequent unfolding. Multiplying 33 translocation cycles by the mean duration of the dwell (~0.35 s) predicts a mean GFP unfolding time of ~11.5 s, which agrees very well with the mean time constant obtained from the distribution of GFP unfolding times, $< \tau > = 11.8 \pm 0.9$ s (Figure S4B; Supplemental Information), as well as from previous single-turnover GFP degradation measurements (Martin et al., 2008b).

At [ATP] ~K_m, ClpXP moves in bursts of at most 3 nm, which may be sufficient to promote the extraction of β11 from the GFP barrel (ClpX succeeds in carrying out the thermodynamic task) but are too small to prevent the refolding of β11 (ClpX fails to accomplish the kinetic task). Thus, under subsaturating ATP conditions, the kinetic competition between ClpXP attempts to translocate the unfolded region and the tendency of that region to refold greatly reduces the unfolding efficiency of the motor.

DISCUSSION

Force Generation in ClpXP Is Coupled to Phosphate Release

Here, we propose a mechanochemical model for ClpXP that identifies the force-generating step in the chemical cycle of ATP hydrolysis (Figure 6A). As shown above, our results revealed that all transitions reversibly connected to ATP binding up to and including the first irreversible step are not involved in force generation. Furthermore, the first irreversible transition in other molecular motors has been identified as the tight binding of ATP (Adachi et al., 2007; Chemla et al., 2005). Indeed, the duration of the ATPγS-induced pauses makes the tight binding of ATP a likely candidate for the first irreversible transition in the mechanochemical cycle of ClpXP. Because tight ATP binding is apparently not rate limiting during translocation, its rate constant (k_{TB}) can be estimated by using a lower bound that corresponds to the translocation rate of the motor, $k_{cat} = 9\ s^{-1}$. The reverse transition from tight to loose binding, k_{-TB}, is given as the inverse of the mean ATPγS-pause duration, ~0.6 s^{-1}. Thus, we obtain a $k_{TB}/k_{-TB} = 15$ and a corresponding free energy change associated with tight binding $\Delta G_{TB} > 2.7\ k_BT$. The tight binding of ATP can therefore be considered the first irreversible transition following ATP binding. As described above, our results exclude the possibility of ATP hydrolysis and ADP release being coupled to the force-generating step and reveal instead that force generation likely occurs upon Pi release. Interestingly, in this aspect ClpX resembles other members of the ASCE family, such as the φ29 DNA-packaging motor and F1-ATPase, harnessing Pi release as a force-generating step despite the distinct architectures and functions within this large family of motors (Chemla et al., 2005).

Intersubunit Coordination Determines the ClpX Translocation Mechanism

Titrations with the slowly hydrolyzable analog ATPγS as well as the analyses of burst sizes and dwell times have revealed several aspects of the intersubunit coordination in the ClpX hexamer. The pause-density dependence on ATPγS concentration suggests that ClpX maintains operation even when one or two

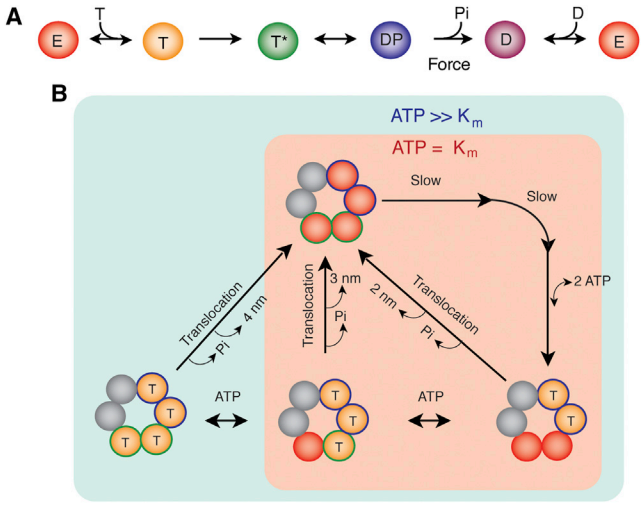

Figure 6. Minimal Mechanochemical Model of ClpXP Translocation

(A) The pathway of ATP hydrolysis for a single subunit of ClpX. An empty subunit (E, red sphere) binds ATP (T, orange) and undergoes a tight binding of ATP (T*, green). Then, the subunit hydrolyzes ATP to ADP and Pi (DP, blue), the force-generation step occurs upon phosphate release (D, purple), and ADP dissociates, leaving an empty subunit (E, red sphere).

(B) Schematic depiction of intersubunit coordination at saturating (green box) and limiting ATP concentrations (red box) for one possible scenario depicting sequential ATP binding. The subunits in gray correspond to those that do not bind ATP. During the dwell phase, at least two ATPs are bound to the high-affinity subunits (T, blue outline), and additional ATPs can bind to the low-affinity ClpX subunits (T, green outline), depending on [ATP]. During the burst phase, the motor hydrolyzes all bound ATPs, releases phosphate, and translocates the substrate by 2, 3, or 4 nm into the central pore.

ATPγS molecules bind to the ring. At least three ATPγS molecules must bind to the ring in order to stall the motor. Based on previous biochemical and structural studies, at most four subunits in the hexamer can bind nucleotide (Hersch et al., 2005; Glynn et al., 2009; Stinson et al., 2013). Because binding of three analog molecules stalls the motor, the remaining fourth subunit may bind ATP but would still be unable to drive translocation. This analysis suggests that the minimal operational unit for substrate translocation by ClpX involves at least two subunits.

That it takes binding of three analog molecules to stall translocation by the ClpX hexamer rules out models of strict intersubunit coordination described previously for other molecular motors (Lyubimov et al., 2011). For instance, it excludes models of concerted hydrolysis, where the subunit power strokes occur simultaneously after all subunits have been loaded with nucleotide. It also contradicts strictly sequential hydrolysis models, in which the power stroke of one subunit occurs only after the power stroke of its neighbor. If one of these models of intersubunit coordination were to apply to ClpX, a single ATPγS binding event would be sufficient to stall the motor. Furthermore, our data are also inconsistent with stochastic or probabilistic hydrolysis models, where all subunits act independently from each other. In a stochastic scenario, all the active subunits would have to bind ATPγS in order to stall translocation. Thus, we find that the ATPase cycles of individual ClpX subunits are neither strictly coordinated nor completely independent from each other. Instead, as will be discussed below, we find that two, three, or four subunits can coordinate their activity in each cycle, depending on the number of ATPs bound to the motor.

The analysis of burst sizes provides direct evidence for how many subunits participate in translocation during a single burst phase. The ClpX crystal structure reveals a distance of 1 nm between the pore loops of adjacent subunits in different nucleotide states, suggesting a 1 nm power stroke per hydrolyzing subunit during substrate translocation (Glynn et al., 2009). Furthermore, dividing the maximum translocation velocity, V_{max} = 8.5 nm/s, by the rate of ATP hydrolysis, k_{cat} = 8.3 ATP s^{-1}, yields 1.02 ± 0.03 nm per hydrolyzed ATP. Thus, if one ATP is hydrolyzed per ClpX subunit, the fundamental translocation step size must be ~1 nm, consistent with previous single-molecule reports (Aubin-Tam et al., 2011; Maillard et al., 2011). Consequently, the variable burst sizes of 2, 3, or 4 nm observed at various ATP concentrations reflect the near-instantaneous, coordinated firing of two, three, or four subunits around the ring. The maximum burst size of 4 nm suggests that up to four subunits in the hexamer participate during a single translocation cycle. The smallest observed burst size as well as the minimum number of ATPγS molecules required to stall the motor allow us to propose that active translocation requires a minimum number of two coordinated subunits.

Surprisingly, our data reveal that bursts of 2 or 3 nm occur much more frequently than bursts of 4 nm, even at saturating concentrations of ATP, suggesting that the most relevant translocation cycle of the ClpX motor involves the coordinated hydrolysis and conformational change of two or three subunits. These results thus provide direct evidence for the operational flexibility of ClpX during polypeptide translocation. Previous bulk biochemical assays and crystal structures of ClpX (Hersch et al., 2005; Glynn et al., 2009; Stinson et al., 2013) revealed hexamers bound to four nucleotides. These findings most likely reflect the state of the ring preceding a 4 nm burst, a state that, in view of our results, is only one of a larger ensemble of nucleotide-bound configurations. Future structural studies in the presence of substrate may capture ClpX loaded with two or three ATP molecules, which according to our data correspond to conformational states that are more probable during polypeptide translocation.

Our results show that the number of subunits participating in a single translocation cycle depends on the availability of ATP. When the ATP concentration was lowered from saturating to near K_m, we observed a redistribution of burst sizes from 3 and 4 nm to 2 and 3 nm. The predominant population of 2 nm bursts and the almost complete absence of 1 nm bursts indicates that, even at partly rate-limiting ATP concentrations ([ATP] ~35 μM), at least two of the subunits must bind ATP in order to initiate a translocation cycle. Therefore, the K_m of these two subunits that bind ATP first must be significantly lower than the average K_m of 35 μM. The lack of 4 nm bursts at ATP concentrations near 35 μM indicates that the remaining subunits have a higher K_m than the first two high-affinity sites and thus contribute to translocation only at high ATP concentrations.

Two different classes of ATP binding sites with correspondingly different binding affinities have been previously identified in ClpX using traditional nucleotide competition assays (Hersch

et al., 2005). Furthermore, recent mutational studies of ClpX have shown strong evidence for a dynamic mechanism of subunit switching, whereby nucleotide binding can affect the affinities of the remaining subunits within the ring (Stinson et al., 2013). Our data shed light onto how the coexistence of subunits with high and low ATP affinity affects the dynamics of the translocation cycle, allowing the burst phase to be initiated with either two ATPs (both binding to high-affinity subunits), three ATPs (two high- and one low-affinity subunits), or four ATPs (two high- and two low-affinity subunits) bound to the motor.

A surprising finding is that, regardless of the number of subunits participating in the translocation cycle, the mean cycle time remains constant for ATP concentrations between $\sim K_m$ and saturating. The mean cycle time is expected to increase when ATP binding becomes rate limiting, and, to probe this behavior, we would have to monitor translocation in the presence of ATP concentrations at or below the K_m for the high-affinity subunits (K_m << 35 μM). However, no translocation activity was observed for ATP concentrations below ~29 μM. Within the accessible ATP-concentration range, we found that the dwell duration is governed by at least two non-ATP-binding events ($n_{min} \sim 2$). The nonbinding events in the dwell could correspond to conformational changes within the ClpX ring that either (1) result from or (2) are completely independent of ATP binding.

An "Internal Clock" Triggers Polypeptide Translocation

Our results provide a model to rationalize the observed invariant dwell-time distribution and the variable burst-size distribution of ClpX as a function ATP concentration. The dwell duration is largely determined by two slow, non-ATP-binding events. By the time these slow transitions occur, the two high-affinity subunits are ATP bound and, depending on the ATP concentration, one or two of the low-affinity subunits are occupied with ATP as well. Due to the constrained ring geometry, only four of the six subunits can be ATP bound (Hwang and Lang, 2013), which provides an explanation for why we do not observe bursts of more than 4 nm even at saturating ATP concentrations. After the motor hydrolyzes all of the bound ATP molecules, Pi release and concomitant subunit power strokes occur near simultaneously around the ring, resulting in a burst size that is proportional to the number of hydrolyzed ATP molecules. The essence of this model is that the mean duration of the dwell phase is constant and set by an "internal signal" or "clock," which may or may not follow ATP binding and could, for instance, correspond to the reaching of a strain threshold in the ring or the hydrolysis of the first-bound ATP. In contrast to this constant average dwell phase, the burst size is variable and proportional to the number of subunits bound to ATP before the clock triggers the initiation of a translocation cycle around the ring. As a result, the ClpXP motor operates at a constant frequency (fixed "rpm") and a variable burst size (different "gears"). Although our current model, depicted in Figure 6B, suggests a spatial and temporal order of ATP-docking events, future single-molecule studies of ClpX mutants will be required to definitively establish the order of ATP-binding and hydrolysis events around the hexameric ring.

Biological Implications of the ClpX Translocation Mechanism

The model proposed here provides a framework to understand how ClpXP successfully unfolds stable protein substrates. The ability of the motor to bind four ATP molecules allows it to translocate in large bursts and thus destabilize and rapidly trap partially unfolded intermediates. For instance, to successfully unfold GFP, ClpX subunits must near-simultaneously take a 4 nm burst, which results in the extraction and translocation of β11 from GFP before this strand can refold onto the β barrel. At saturating concentrations of ATP, the time required for ClpX-induced unfolding of GFP is determined by the time that passes before the motor makes a 4 nm burst. In contrast, ClpX rarely unfolds GFP at ATP concentrations near K_m because hydrolysis under these conditions is always triggered before four ATP molecules can bind to the motor. In support of our finding, previous biochemical studies have shown a nonlinear decrease in GFP degradation with decreasing ATPase rate (Martin et al., 2008b), whereas a linear correlation emerges for circular permutants of GFP that do not form a stable unfolding intermediate upon extraction of their C-terminal β strand (Nager et al., 2011). Our results reveal that the decreased probability of the motor taking a 4 nm burst (from ~20% at saturating [ATP] to ~0% at [ATP] near K_m) is responsible for the observed nonlinear decrease of GFP unfolding probability with the ATPase rate.

Based on bulk biochemical studies, it has recently been suggested that the ClpX motor may operate by a partially probabilistic mechanism during unfolding and translocation (Stinson et al., 2013). Our results show that ClpX translocates substrates using a highly coordinated mechanism in which, regardless of the number of translocating subunits, the average dwell duration is constant and followed by a variable burst size that reflects the firing of a different number of subunits in rapid succession. Although there is a stochastic element during the loading of ATP, we observe a high degree of intersubunit coordination during the rapid burst phase of translocation.

Such a mechanism of a constant cycle time (resulting in a variable burst size) allows flexibility for ClpX to successfully overcome unique chemical and mechanical obstacles during polypeptide translocation. A constant cycle time governed by an internal clock provides the motor with a fail-safe mechanism to drive translocation even when some subunits are not loaded with nucleotide. This characteristic will allow the motor to prevent substrate disengagement or prolonged periods of stalling during unfolding attempts when a subset of subunits is unable to maintain grip on the polypeptide.

Our results thus provide an archetype of molecular-motor operation that differs significantly from those described previously for other ring-shaped motors. For instance, the translocation mechanism of the φ29 DNA packaging ATPase requires that periodic contacts be made by the motor every 10 bp along the helical pitch of double-stranded DNA. In order to achieve a fixed burst size of 10 bp, the motor must wait during the dwell until all subunits are loaded with ATP. This mode of operation may have been optimized to keep the motor in register with the symmetry of its DNA substrate and provides a fascinating contrast to our results on ClpX. Because a polypeptide track is aperiodic, ClpX cannot rely on contacting a regularly repeating motif, and

its variable burst size (different "gears") and constant cycle time (constant "rpm") may have arisen as a flexible mechanism that optimizes its efficiency for robust kinetic trapping of unfolding intermediates. The distinction between these mechanisms offers clear evidence for the evolutionary constraints imposed by the motor's substrates to favor certain mechanisms of operation. The mechanisms described here thus provide important insights into the operating principles of ATP-dependent proteases and may have critical implications for the understanding of other ring-shaped ATPases of the AAA+ and RecA families in general.

EXPERIMENTAL PROCEDURES

Sample Preparation

Biotinylated ClpX single-chain hexamers, GFP-titin^{CM} I27 fusion proteins, and 3 kbp dsDNA handle for protein attached via ybbR tag/Sfp system were prepared as described previously (Maillard et al., 2011; Martin et al., 2005, 2008a). Tethers were assembled in a buffer (25 mM HEPES-KCl [pH 7.4], 20 mM $MgCl_2$, 100 mM KCl, and 0.5 mM EDTA) supplemented with (1) [ATP] = 35 μM, 45 μM, 100 μM, 200 μM, 0.5 mM, 1 mM, and 5 mM with ATP regeneration system (Kenniston et al., 2003), (2) [ADP] = 10 μM, 20 μM, 50 μM, 100 μM, and 250 μM in the presence of [ATP] = 100 μM, 200 μM, 500 μM, 1,000 μM and [Pi] = 5 μM, (3) 5 μM, 5 mM, 10 mM $NaPO_4$ (Sigma), (4) [ATPγS] = 25 μM, 50 μM, 100 μM, 175 μM, and 250 μM (Roche) in the presence of [ATP] = 500 μM. All single-molecule experiments required 500 nM of ClpP for the formation of the ClpXP complex (K_d = 90 nM) (Joshi et al., 2004).

Data Collection

Two different dual-trap optical trapping instruments with 1,064 nm laser were employed (Moffitt et al., 2006). The unfolded polypeptide contour length was calculated as previously described (Bustamante et al., 1994; Cecconi et al., 2005; Maillard et al., 2011). Using 0.9 μm polystyrene beads, an oxygen scavenging system was added to prevent the formation of the reactive species singlet oxygen (100 mg/ml glucose oxidase, 20 mg/ml catalase, 5 mg/ml dextrose; Sigma-Aldrich) (Moffitt et al., 2009).

Analysis

Pauses were removed from velocity using a previously described modified Kalafut-Visscher (KV) algorithm with a pause threshold and penalty (Kalafut and Visscher, 2008; Chistol et al., 2012). A cutoff threshold was calculated by taking three SDs of a gamma-fitted distribution. Velocity was calculated as the end-to-end distance Δx/Δt. To calculate pause-free velocity, the selected pauses were removed in the Δt component. Furthermore, we analyzed the pause density and frequency of ATPγS using the modified KV algorithm. ATPγS-induced pauses were extracted by removing ATP-only dwells using a double exponential fit with one time constant fixed to the mean dwell duration measured at saturating [ATP]. Steps and dwells were analyzed using pairwise distribution and t test (Moffitt et al., 2009). Data were filtered to 15–25 Hz and binned into 0.3 and 0.4 nm for the pairwise distributions. The unfolding events and its related measurements were measured by a previously described method (Maillard et al., 2011).

SUPPLEMENTAL INFORMATION

Supplemental Information includes Extended Experimental Procedures and four figures and can be found with this article online at http://dx.doi.org/10.1016/j.cell.2013.09.022.

ACKNOWLEDGMENTS

We thank Shixin Liu, Gheorghe Chistol, Ninning Liu, Christian Kaiser, and Mary Matyskiela for helpful discussions. M.S. and K.N. acknowledge support from the NSF Graduate Research Fellowship. This research was supported in part by the Searle Scholars Program (A.M.), the NIH grant R01-GM094497-01A1 (A.M.), the NIH grant R01-GM0325543 (C.B.), the U.S. Department of Energy, Office of Basic Energy Sciences, Division of Materials Sciences and Engineering under contract no. DE-AC02-05CH11231 (C.B.), and the Howard Hughes Medical Institute (C.B.).

Received: March 9, 2013
Revised: August 9, 2013
Accepted: September 11, 2013
Published: October 24, 2013

REFERENCES

Adachi, K., Oiwa, K., Nishizaka, T., Furuike, S., Noji, H., Itoh, H., Yoshida, M., and Kinosita, K., Jr. (2007). Coupling of rotation and catalysis in F(1)-ATPase revealed by single-molecule imaging and manipulation. Cell *130*, 309–321.

Aubin-Tam, M.E., Olivares, A.O., Sauer, R.T., Baker, T.A., and Lang, M.J. (2011). Single-molecule protein unfolding and translocation by an ATP-fueled proteolytic machine. Cell *145*, 257–267.

Baker, T.A., and Sauer, R.T. (2006). ATP-dependent proteases of bacteria: recognition logic and operating principles. Trends Biochem. Sci. *31*, 647–653.

Baker, T.A., and Sauer, R.T. (2012). ClpXP, an ATP-powered unfolding and protein-degradation machine. Biochim. Biophys. Acta *1823*, 15–28.

Burton, R.E., Baker, T.A., and Sauer, R.T. (2003). Energy-dependent degradation: Linkage between ClpX-catalyzed nucleotide hydrolysis and protein-substrate processing. Protein Sci. *12*, 893–902.

Bustamante, C., Marko, J.F., Siggia, E.D., and Smith, S. (1994). Entropic elasticity of lambda-phage DNA. Science *265*, 1599–1600.

Cecconi, C., Shank, E.A., Bustamante, C., and Marqusee, S. (2005). Direct observation of the three-state folding of a single protein molecule. Science *309*, 2057–2060.

Chemla, Y.R., Aathavan, K., Michaelis, J., Grimes, S., Jardine, P.J., Anderson, D.L., and Bustamante, C. (2005). Mechanism of force generation of a viral DNA packaging motor. Cell *122*, 683–692.

Chistol, G., Liu, S., Hetherington, C.L., Moffitt, J.R., Grimes, S., Jardine, P.J., and Bustamante, C. (2012). High degree of coordination and division of labor among subunits in a homomeric ring ATPase. Cell *151*, 1017–1028.

Glynn, S.E., Martin, A., Nager, A.R., Baker, T.A., and Sauer, R.T. (2009). Structures of asymmetric ClpX hexamers reveal nucleotide-dependent motions in a AAA+ protein-unfolding machine. Cell *139*, 744–756.

Gottesman, S., Roche, E., Zhou, Y., and Sauer, R.T. (1998). The ClpXP and ClpAP proteases degrade proteins with carboxy-terminal peptide tails added by the SsrA-tagging system. Genes Dev. *12*, 1338–1347.

Hanson, P.I., and Whiteheart, S.W. (2005). AAA+ proteins: have engine, will work. Nat. Rev. Mol. Cell Biol. *6*, 519–529.

Hersch, G.L., Burton, R.E., Bolon, D.N., Baker, T.A., and Sauer, R.T. (2005). Asymmetric interactions of ATP with the AAA+ ClpX6 unfoldase: allosteric control of a protein machine. Cell *121*, 1017–1027.

Hwang, W., and Lang, M.J. (2013). Nucleotide-dependent control of internal strains in ring-shaped AAA+ motors. Cell. Mol. Bioeng. *6*, 65–73.

Joshi, S.A., Hersch, G.L., Baker, T.A., and Sauer, R.T. (2004). Communication between ClpX and ClpP during substrate processing and degradation. Nat. Struct. Mol. Biol. *11*, 404–411.

Kalafut, B., and Visscher, K. (2008). An objective, model-independent method for detection of non-uniform steps in noisy signals. Comput. Phys. Commun. *179*, 716–723.

Keller, D., and Bustamante, C. (2000). The mechanochemistry of molecular motors. Biophys. J. *78*, 541–556.

Kenniston, J.A., Baker, T.A., Fernandez, J.M., and Sauer, R.T. (2003). Linkage between ATP consumption and mechanical unfolding during the protein processing reactions of an AAA+ degradation machine. Cell *114*, 511–520.

King, R.W., Deshaies, R.J., Peters, J.M., and Kirschner, M.W. (1996). How proteolysis drives the cell cycle. Science *274*, 1652–1659.

Lyubimov, A.Y., Strycharska, M., and Berger, J.M. (2011). The nuts and bolts of ring-translocase structure and mechanism. Curr. Opin. Struct. Biol. *21*, 240–248.

Maillard, R.A., Chistol, G., Sen, M., Righini, M., Tan, J., Kaiser, C.M., Hodges, C., Martin, A., and Bustamante, C. (2011). ClpX(P) generates mechanical force to unfold and translocate its protein substrates. Cell *145*, 459–469.

Martin, A., Baker, T.A., and Sauer, R.T. (2005). Rebuilt AAA + motors reveal operating principles for ATP-fuelled machines. Nature *437*, 1115–1120.

Martin, A., Baker, T.A., and Sauer, R.T. (2008a). Pore loops of the AAA+ ClpX machine grip substrates to drive translocation and unfolding. Nat. Struct. Mol. Biol. *15*, 1147–1151.

Martin, A., Baker, T.A., and Sauer, R.T. (2008b). Protein unfolding by a AAA+ protease: critical dependence on ATP-hydrolysis rates and energy landscapes. Nat. Struct. Mol. Biol. *15*, 139–145.

Moffitt, J.R., Chemla, Y.R., Izhaky, D., and Bustamante, C. (2006). Differential detection of dual traps improves the spatial resolution of optical tweezers. Proc. Natl. Acad. Sci. USA *103*, 9006–9011.

Moffitt, J.R., Chemla, Y.R., Aathavan, K., Grimes, S., Jardine, P.J., Anderson, D.L., and Bustamante, C. (2009). Intersubunit coordination in a homomeric ring ATPase. Nature *457*, 446–450.

Nager, A.R., Baker, T.A., and Sauer, R.T. (2011). Stepwise unfolding of a β barrel protein by the AAA+ ClpXP protease. J. Mol. Biol. *413*, 4–16.

Oster, G., and Wang, H. (2000). Reverse engineering a protein: the mechano-chemistry of ATP synthase. Biochim. Biophys. Acta *1458*, 482–510.

Schnitzer, M.J., and Block, S.M. (1995). Statistical kinetics of processive enzymes. Cold Spring Harb. Symp. Quant. Biol. *60*, 793–802.

Segel, I.H. (1975). Enzyme Kinetics (New York: Wiley), pp. 100–141.

Stinson, B.M., Nager, A.R., Glynn, S.E., Schmitz, K.R., Baker, T.A., and Sauer, R.T. (2013). Nucleotide binding and conformational switching in the hexameric ring of a AAA+ machine. Cell *153*, 628–639.

Visscher, K., Schnitzer, M.J., and Block, S.M. (1999). Single kinesin molecules studied with a molecular force clamp. Nature *400*, 184–189.

White, S.R., and Lauring, B. (2007). AAA+ ATPases: achieving diversity of function with conserved machinery. Traffic *8*, 1657–1667.

Yang, F., Moss, L.G., and Phillips, G.N., Jr. (1996). The molecular structure of green fluorescent protein. Nat. Biotechnol. *14*, 1246–1251.